Seedless Polyol Synthesis and CO Oxidation Activity of Monodisperse (111) and (100)-Oriented Rhodium Nanocrystals in Sub-10 nm Sizes

Yawen Zhang,[†‡]* Michael E. Grass,[‡] Wenyu Huang,[‡] and Gabor A. Somorjai[‡]*

[†] *College of Chemistry and Molecular Engineering, and the State Key Lab of Rare Earth Materials Chemistry and Applications & PKU-HKU Joint Lab in Rare Earth Materials and Bioinorganic Chemistry, Peking University, Beijing 100871, China*

[‡] *Department of Chemistry, University of California, Berkeley, California 94720, and the Chemical and Materials Sciences Divisions, Lawrence Berkeley National Laboratory, 1 Cyclotron Road, Berkeley, California 94720*

* Corresponding authors. E-mail: ywzhang@pku.edu.cn; somorjai@berkeley.edu.

Abstract

Monodisperse sub-10 nm (6.5 nm) sized Rh nanocrystals with (111) and (100) surface structures were synthesized by a seedless polyol reduction in ethylene glycol, with poly(vinylpyrrolidone) as a capping ligand. When using $[Rh(Ac)_2]_2$ as the metal precursor, (111)-oriented Rh nanopolyhedra containing 76% (111)-twined hexagons (in 2D projection) were obtained; whereas, when employing $RhCl_3$ as the metal precursor in the presence of alkylammonium bromide, such as tetramethylammonium bromide and trimethyl(tetradecyl)ammonium bromide, (100)-oriented Rh nanocubes were obtained with 85% selectivity. The {100} faces of the Rh nanocrystals are stabilized by chemically adsorbed Br^- ions from alkylammonium bromides, which led to (100)-oriented nanocubes. Monolayer films of the (111)-oriented Rh nanopolyhedra and (100)-oriented Rh nanocubes were deposited on silicon wafers in a Langmuir-Blodgett trough to make model 2D nanoarray catalysts. These nanocatalysts were active for CO oxidation by O_2, and the turnover frequency was independent of nanoparticle shape, consistent with that previously observed for Rh(111) and Rh(100) single crystals.

Introduction

Monodisperse shape-controlled noble metal nanocrystals have considerable scientific and technological significance in the catalytic field.[1,2] Precise shape control may help reveal fundamental catalytic properties of nanoscale materials in comparison with their bulk counterpart (single crystals), as well as provide tunable catalytic activity and selectivity for nanocatalysts in many technologically important heterogeneous reactions.[1,2] Several solution phase syntheses including modified polyol methods,[1a,1g,1k,3a,3b,4,5a,6a,7a] seeded growth by polyol reduction,[7b,c] thermolysis of organometallics,[1f,7d,7e] and micelle techniques[3c,5b,6b] have been developed to kinetically and/or thermodynamically manipulate the shape of noble metal nanocrystals (e.g. Pt,[1a,1f,1k,3] Pd,[4] Ag,[5] Au[6] and Rh[1g,7]), by regulating the relative growth rates along low-index plane directions (i.e. <100> and <111>).

Rh nanocatalysts have been employed in many heterogeneous reactions including hydrogenation,[8a,8e] hydroformylation,[8b] hydrocarbonylation,[8c] and combustion.[8d] Shape control of Rh nanocrystals provides a route for probing how faceting on the nanoscale influences catalytic activity and selectivity. Several groups have been engaged in size and shape control of Rh nanocrystals via various solution chemistry approaches. By a polyol approach, Xia's group prepared Rh multipods that demonstrate useful SERS activity.[7a] With a polyol seeded growth, the Somorjai and Tilley groups obtained crystalline Rh multipods, cubes, horns and cuboctahedra.[7b,c] Through organometallic routes, Son and coworkers synthesized near-monodisperse tetrahedral Rh nanocrystals (displaying shape-dependent catalytic hydrogenation of arenes),[7d] and ultrathin Rh nanoplates at a low temperature.[7e] Liang and coworkers prepared catalytically active shape selective Rh nanocubes through a simple photochemical method.[7f] More recently, Somorjai's group made size-controllable monodisperse (111)-oriented Rh nanocrystals employing a one-step polyol technique,[9] and obtained monodisperse sub-10 nm sized Rh nanocubes in a high selectivity (>85%) by a seedless polyol method.[1g] However, there has thus far been no report on the synthesis of monodisperse Rh nanocrystals at a constant size below 10 nm but with different surface structures by the same synthetic technique, and there is scarce investigation of the shape effects on the catalytic activity and selectivity for those shape-tunable Rh nanocrystals.

In this paper, we report a seedless polyol synthesis of monodisperse sub-10 nm sized Rh nanocrystals with (111) and (100) surface structures in ethylene glycol, using rhodium acetate and rhodium chloride as the

metal precursors. The shape evolution mechanism was carefully explored with various characterization methods including transmission electron microscopy (TEM) and ultraviolet-visible (UV-vis) spectroscopy. The shape evolution from (111)-oriented Rh nanopolyhedra to (100)-oriented Rh nanocubes was demonstrated being induced by the selective adsorption of Br^- ions from akylammonium bromides onto the (100) faces of Rh nanocrystals. Using CO oxidation as a model heterogeneous catalytic reaction, the shape effect on the catalytic activity of the (111) and (100)-orientated Rh nanocrystals was explored, in agreement with previous single crystal studies.

Experimental Section

1. Chemicals. Rhodium(II) acetate dimer powder ([Rh(Ac)$_2$]$_2$, Sigma-Aldrich), rhodium(III) chloride hydrate (RhCl$_3$·xH$_2$O; Sigma-Aldrich), rhodium(III) bromide hydrate (RhBr$_3$·xH$_2$O; Sigma-Aldrich), rhodium(III) acetylacetonate (Rh(acac)$_3$, 97%, Sigma-Aldrich), poly(vinylpyrrolidone) (PVP, Mw = 24,000 and 55,000; Sigma-Aldrich), tetramethylammonium bromide (TMAB, (CH$_3$)$_4$N$^+$Br$^-$, $\geqslant$98.0%, Sigma-Aldrich), tetraethylammonium bromide (TEAB, (C$_2$H$_5$)$_4$N$^+$Br$^-$, 98.0%, Sigma-Aldrich), trimethyldodecylammonium bromide (TDAB, (C$_{12}$H$_{25}$)N$^+$(CH$_3$)$_3$Br$^-$, 99%; Sigma-Aldrich), trimethyl(tetradecyl)ammonium bromide (TTAB, (C$_{14}$H$_{29}$)N$^+$(CH$_3$)$_3$Br$^-$, 99%; Sigma-Aldrich), ethylene glycol (>98%; EMD), and solvents (analytical grade) including acetone, ethanol, hexanes and chloroform were used without further purification.

2. Synthesis of (111)-Oriented Rh Nanopolyhedra. 0.00625 mmol [Rh(Ac)$_2$]$_2$ and 0.25 mmol poly(vinylpyrrolidone) (Mw = 55,000, in terms of the repeating unit) were added to 20 ml ethylene glycol in a 50 ml three-necked flask at room temperature. The stock solution was heated to 100 °C in a Glas-Col electromantle (60 W; 50 ml) with a Cole-Parmer temperature controller (Diqi-sense®), and was evacuated at this temperature for 20 min to remove water and oxygen under magnetic stirring, resulting in a green solution. The flask was then heated to 185 °C at 10 °C min^{-1}, and maintained at this temperature for 2 h under Ar. When the reaction was complete, an excess of acetone was added at room temperature to form a cloudy black suspension. This suspension was separated by centrifugation at 4200 rpm for 6 min, and the black product was collected by discarding the colorless supernatant. The precipitated Rh nanocrystals were

washed twice by precipitation/dispersion (re-dispersed in 7.5 ml of ethanol with sonication and then precipitated by adding 37.5 ml of hexanes).

Synthesis of (100)-Oriented Rh nanocubes. The synthetic procedure of Rh nanocubes was the same as that used to synthesize Rh nanopolyhedra, except that 0.2 mmol $RhCl_3$, 1 mmol tetramethylammonium bromide, and 4 mmol poly(vinylpyrrolidone) (Mw = 24,000, in terms of the repeating unit) were added to 20 ml ethylene glycol in a 50 ml three-necked flask at room temperature, which was evacuated at 80 °C for 20 min, and heated at 185 °C for 1.5 h.

3. Fabrication of Langmuir-Blodgett (LB) Films. The Rh nanocrystals were washed several times by precipitation/dispersion in ethanol and then in chloroform (1 ml Rh suspension was precipitated by adding 4 ml of hexane, and re-dispersed in 1 ml of ethanol or chloroform with sonication), to remove impurities and excess PVP. Monolayers of Rh nanocrystals were formed by placing drops of Rh nanocrystal chloroform solution onto the water subphase of a LB trough (Nima Technology, M611) at room temperature.[1g,3a,9] The surface pressure was monitored with a Wilhelmy plate, and was adjusted to zero before spreading the nanocrystals. The resulting surface layer was compressed by moving the mobile barrier at a rate of 15 cm^2 min^{-1}. At different stages of compression, the Rh layers at the water-air interface were carefully transferred onto continuous carbon-coated copper grids using the Langmuir-Schäffer horizontal liftoff method. The surface coverage was evaluated by measuring the particle coverage on selected areas of the TEM grids. The Rh nanocrystals were deposited onto Si wafers (1 cm × 1 cm) by lift-up of the substrates at a rate of 1 mm min^{-1}.

4. Characterization Methods. The shape, size and lattice structure of the Rh nanocrystals were analyzed using a Philips FEI Tecnai 12 Transmission electron microscope (TEM) and Philips CM200/FEG high-resolution TEM (HRTEM), operated at 100 and 200 kV, respectively. The samples were prepared by placing a drop of Rh nanocrystal sol in ethanol onto a continuous carbon-coated copper TEM grid. The size and shape distribution of the Rh nanocrystals are reported from analysis of at least 50 particles. Powder X-ray diffraction (XRD) patterns were recorded on a Bruker D8 GADDS diffractometer using Co-K$_a$ radiation (λ = 1.79 Å). All UV-vis absorption spectra were measured on an Agilent 8453 UV-visible ChemStation

equipped with a 1 cm path length quartz cuvette, using samples prepared by diluting 0.1 ml of reaction solution (aspirated directly from the reaction system with a 1 ml plastic syringe) with 5 ml absolute ethanol.

5. CO Oxidation. CO oxidation reactions were performed in a laboratory scale batch reactor with continuous gas recirculation between 170 and 230 °C. Samples were loaded into quartz reactors with a type-K thermocouple touching the reactor near the sample. Prior to the reaction, the manifold was filled with 40 Torr CO (Praxair, UHP), 100 Torr O_2 (Praxair, UHP), and a balance of He (Praxair, UHP) initially at atmospheric pressure, all regulated by mass flow controllers. Gas composition was analyzed with a HP 5890 Series II gas chromatograph (GC) equipped with a thermal conductivity (TCD) and a flame ionization (FID) detector. Turnover frequency (TOF) was calculated by extrapolating the conversion data to the initial time and by correcting the Rh surface area for coverage from TEM, and for shape (assuming non-overlapping cubic particles).

Results and Discussion

1. Characterization of (111) and (100)-Oriented Rh Nanocrystals.
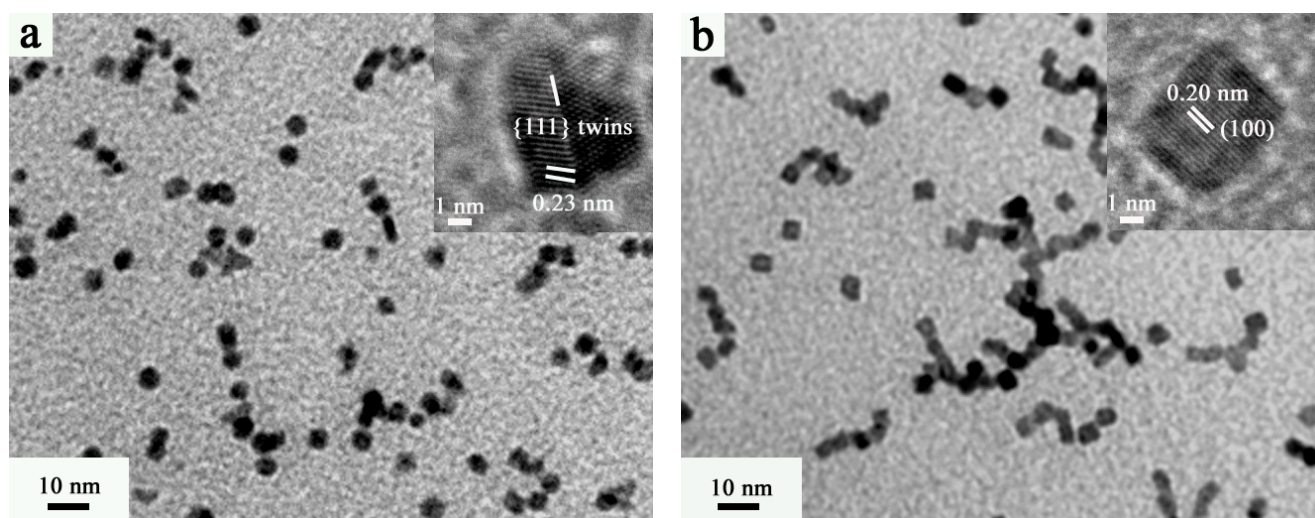
Figure 1. TEM and HRTEM (inset) images of Rh (a) nanopolyhedra and (b) nanocubes synthesized in 20 ml ethylene glycol under an Ar atmosphere: (a) 0.3125 mM [Rh(Ac)$_2$]$_2$, 12.5 mM PVP, 185 °C, 2 h; (b) 10 mM RhCl$_3$, 50 mM TMAB, 200 mM PVP, 185 °C, 1.5 h.

We prepared (111)-oriented Rh nanopolyhedra, and (100)-oriented Rh nanocubes in a size around 6.5 nm using a seedless polyol method. As seen from the TEM images shown in Figures 1, S1a and S1c, the Rh nanopolyhedra and nanocubes are monodisperse, with sizes of 6.5±0.6 and 6.2 ±0.6 nm, respectively. The Rh nanopolyhedra (as observed in 2D projection) are composed of 76% hexagons (twinned particles), 8% triangles ((111)-oriented tetrahedra), 11% squares ((100)-oriented cubes) and 5% irregular particles (Figures 1a and S1a). The inset in Figure 1a shows a representative HRTEM image of a crystalline hexagon, which is a single twinned particle exposing {111} planes (interplanar distance: 0.23 nm). The nanocube sample contains 85% cubes and 15% irregular particles (Figures 1b and S1c). The inset in Figure 1b shows a typical HRTEM image of a single-crystalline cube exposing six {100} planes (interplanar distance: 0.20 nm).
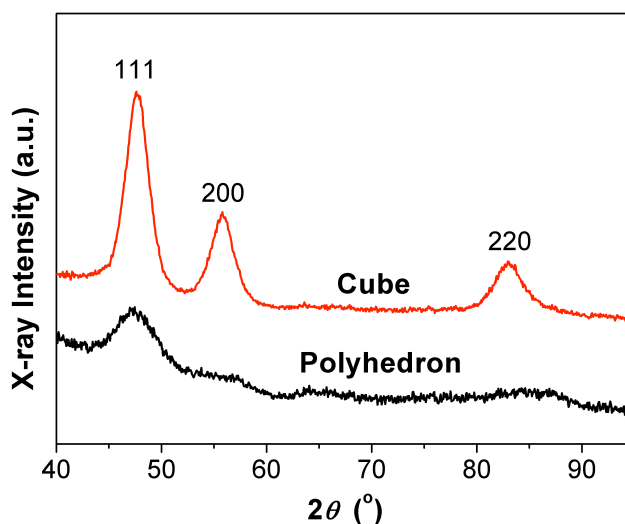
Figure 2. XRD patterns of Rh nanopolyhedra and nanocubes.

XRD measurement revealed that both the Rh nanopolyhedra and Rh nanocubes adopt a face-centered-cubic (fcc) structure with calculated constants of 0.379 and 0.382 nm (JCPDS: 5-685), respectively. Because of the highly-strained nature and multiply twining of the small fcc structured noble metal nanoparticles,[10] the line width of the (111) peak for the Rh nanopolyhedra is considerably broader than that for the Rh nanocubes. The ratio of $I_{(111)}/I_{(200)}$ for the Rh nanopolyhedra is 5.3, nearly double of that (2.3) for the Rh nanocubes, indicative of their different surface structures, as also determined from the above HRTEM measurements.
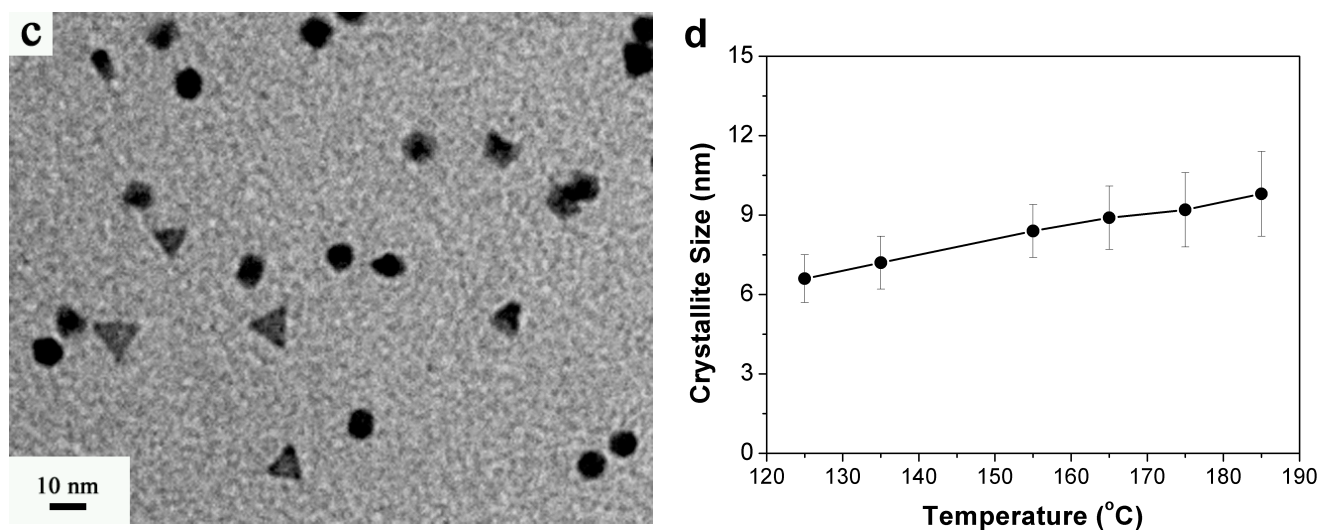
2. Formation of (111)-Oriented Rh Nanocrystals.
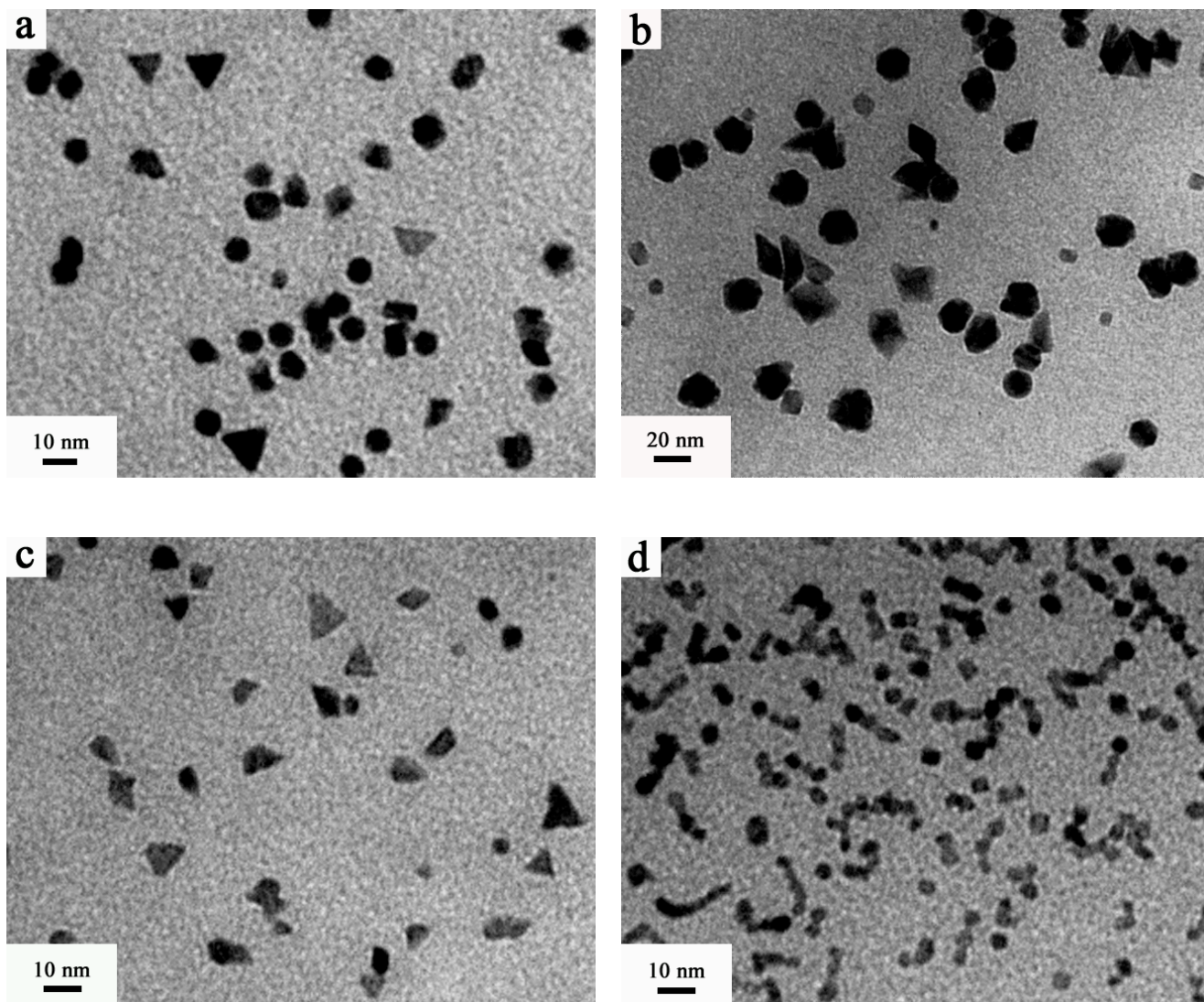
Figure 3. TEM images of Rh nanocrystals synthesized in 20 ml ethylene glycol under an Ar atmosphere: (a) 2.5 mM [Rh(Ac)$_2$]$_2$, 100 mM PVP, 185 °C, 2 h; (b) 5 mM Rh(acac)$_3$, 50 mM PVP, 185 °C, 3 h; (c) 5 mM RhCl$_3$, 50 mM PVP, 185 °C, 2 h; (d) 5 mM RhBr$_3$, 50 mM PVP, 185 °C, 2 h.

Precursor Effect. The Rh precursor has a large influence on the shape and monodispersity of nanocrystals synthesized in ethylene glycol. At 185 °C, the use of 2.5 mM [Rh(Ac)$_2$]$_2$ for a 2 h reaction yielded near-monodisperse Rh nanopolyhedra (40% hexagons, 14% pentagons ((111)-twinned decahedra), 25% triangles, 8% squares, and 12% irregular particles) (9.8±1.6 nm; Figures 3a and S1b). The reaction of Rh(acac)$_3$ at 185 °C for 3 h formed highly polydisperse Rh nanopolyhedra (31% hexagons, 16% pentagons, 12% triangles, 22% squares, and 19% irregular particles) (16.9 ±6.2 nm; Figure 3b). The use of RhCl$_3$ for a 2 h reaction at 185 °C produced polydisperse Rh nanocrystals (30% triangles, 4% squares, and 66% irregular particles) (8.0 ±2.0 nm; Figure 3c); whereas employing RhBr$_3$ under otherwise identical reaction conditions, near-monodisperse Rh nanocrystals containing more nanocubes (41% squares and 59% irregular particles) were obtained (5.6±0.8 nm; Figure 3d). These results suggest that [Rh(Ac)$_2$]$_2$ is the best precursor for the formation of monodisperse (111)-oriented Rh nanopolyhedra in ethylene glycol, and the introduction of Br ions into the synthesis enhances the selectivity towards (100)-oriented Rh nanocubes of a smaller size.[1g]
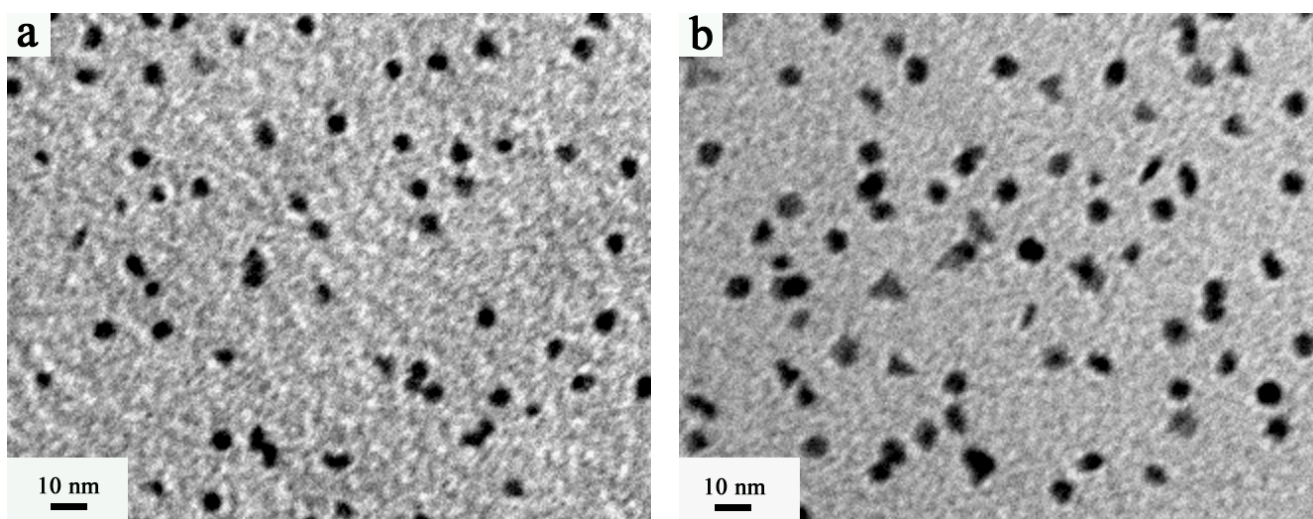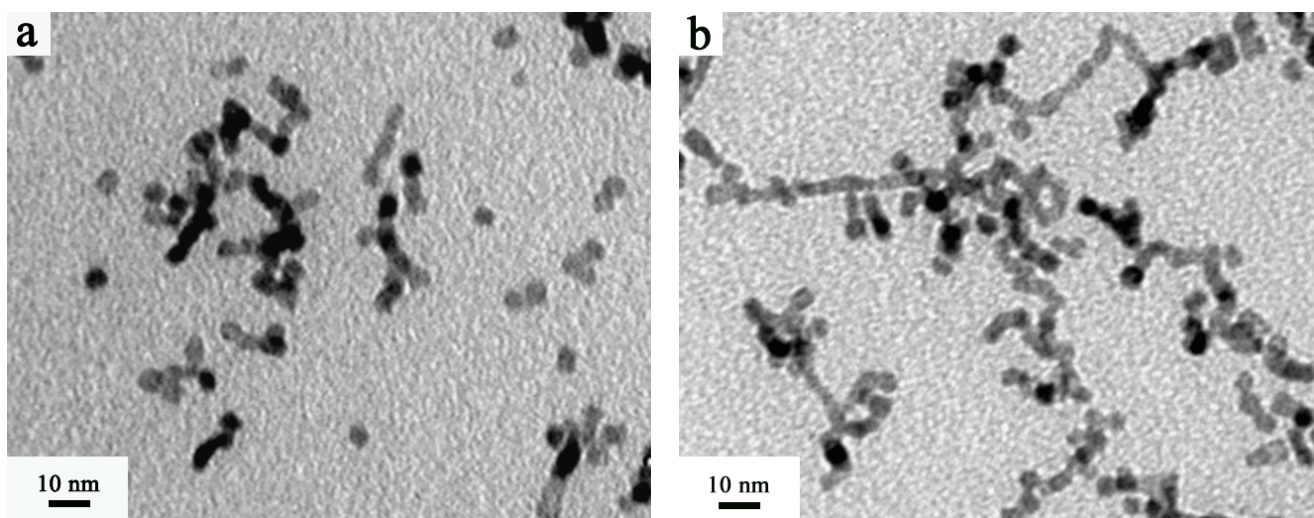
Figure 4. TEM images of Rh nanopolyhedra synthesized in 20 ml ethylene glycol under an Ar atmosphere at different temperatures for 2 h, using 2.5 mM [Rh(Ac)$_2$]$_2$ and 100 mM PVP: (a) 125 °C; (b) 135 °C; (c) 165 °C. (d) Crystallite size of the Rh nanopolyhedra as a function of synthetic temperature.

Temperature Effect. The reduction of 2.5 mM [Rh(Ac)$_2$]$_2$ at 125 °C for 2 h by ethylene glycol resulted in 6.6 ±0.9 nm Rh nanocrystals (Figure 4a,d). At 135 °C, the nanocrystals were larger (7.2 ±1.0 nm) and demonstrated improved faceting (Figure 4b,d). With a further increase in reaction temperature, the size of the Rh nanocrystals increased to 8.4 ±1.0 nm (155 °C) and 8.9 ±1.2 nm (165 °C) (Figure 4c,d). At these elevated temperatures, the nanocrystals were highly-faceted with well-defined shapes (Figure 4c) (30% hexagons, 15% pentagons, 17% triangles, 11% squares, and 27% irregular particles). Upon further increase in reaction temperature to 175 °C and 185 °C, well-shaped 9.2 ±1.4 (Figure 4d) and 9.8 ±1.8 nm (Figure 3a) Rh nanocrystals, respectively, were obtained. It is noteworthy that the standard deviations of the size distributions for the Rh nanocrystals are all around 15% in the temperature range of 125-185 °C (Figure 4d). Increasing reaction temperature results in an increase in the size of the nanocrystals and also promotes the faceting of Rh nanocrystals by developing well-defined edges and corners.

3. Formation of (100)-Oriented Rh Nanocrystals.

Effect of Alkylammonium Bromide. It has been demonstrated that, when using RhCl$_3$ as the metal precursor, Br$^-$ ions from various alkylammonium bromides effectively stabilize the {100} faces of Rh

10

nanocrystals, and induces the evolution of nanocubes. 6.2 ± 0.6, 6.4 ± 0.5, 6.1 ± 0.6, and 6.4 ± 0.5 nm Rh nanocubes with greater than 85% selectivity were formed from TMAB (85% cubes and 15% irregular particles; Figure 1b), TEAB (85% cubes and 15% irregular particles; Figure 5a), TDAB (87% cubes and 13% irregular particles; Figure 5b) and TTAB (86% cubes and 15% truncated cubes; Figures 5c,S1d). This suggests that the formation of Rh nanocubes is due to the stabilization of {100} planes by chemically adsorbed Br$^-$ ions, rather than by interactions between the organic ammonium cations and the nanocrystal surfaces. The adsorption of Br species on to the nanocube surface was confirmed by EDS analysis.[1g] Further, it is observed that the Rh nanocubes prepared from TTAB exhibited well-defined edges and corners (Figures 5c,S1d). As the concentration of RhCl$_3$ and TTAB was decreased by half, slightly truncated 5.8 ± 0.6 nm Rh nanocubes of decreased selectivity (61% cubes and 39% irregular particles) were obtained (Figure 5d), possibly owing to the minimization effect of the total surface energy for small nanoparticles.[2c]
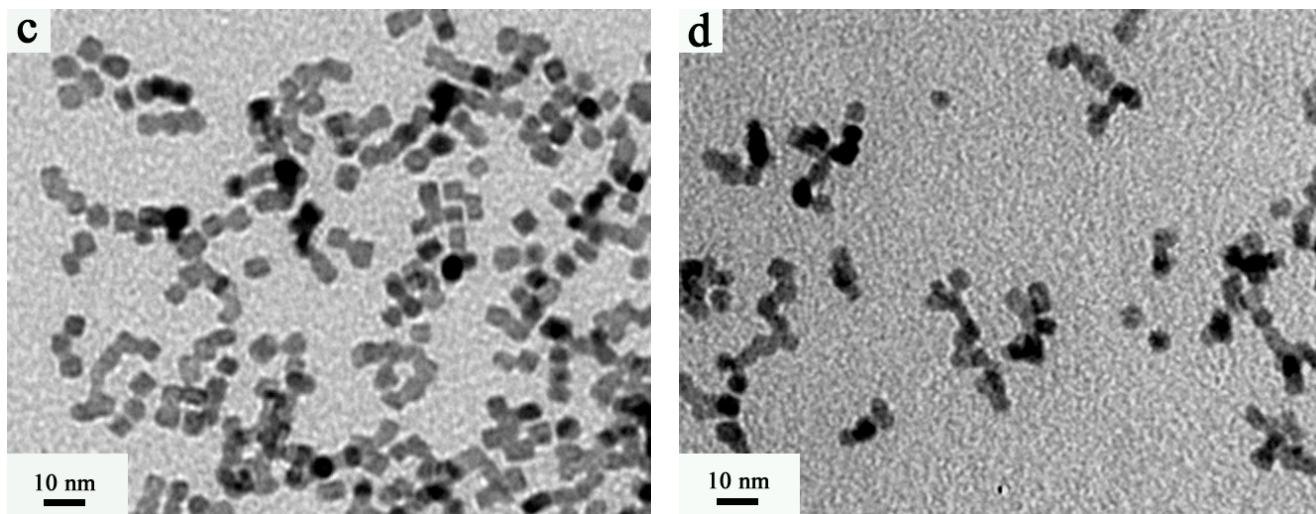
Figure 5. TEM images of Rh nanocrystals synthesized in 20 ml ethylene glycol under an Ar atmosphere at 185 °C for 1.5 h: (a) 10 mM RhCl$_3$, 50 mM TEAB, 200 mM PVP; (b) 10 mM RhCl$_3$, 50 mM TDAB, 200 mM PVP; (c) 10 mM RhCl$_3$, 50 mM TTAB, 200 mM PVP; (d) 5 mM RhCl$_3$, 25 mM TTAB, 100 mM PVP.
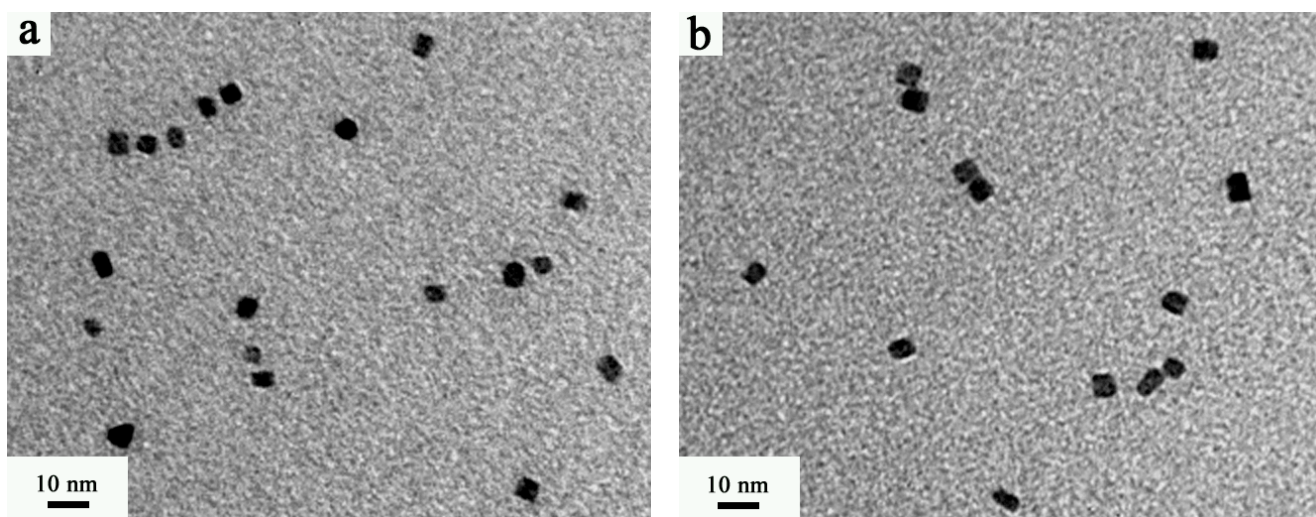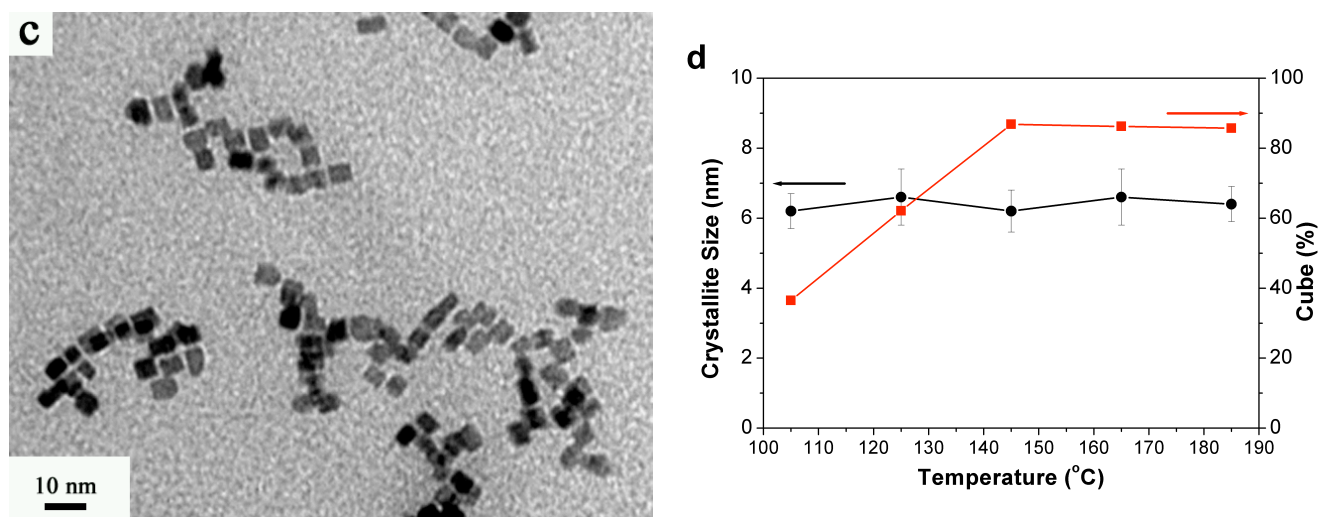
Figure 6. TEM images of Rh nanocubes synthesized in 20 ml ethylene glycol under an Ar atmosphere at different temperatures for 1.5 h, using 10 mM RhCl$_3$, 50 mM TTAB and 200 mM PVP: (a) 105 °C; (b) 125 °C; (c) 145 °C. (d) Crystallite size of the Rh nanocubes as a function of synthetic temperature.

Temperature Effect. At a set concentration of 10 mM RhCl$_3$ and 50 mM TTAB, 6.2 ± 0.5, 6.6 ± 0.8, 6.2 ± 0.6, 6.6 ± 0.8, and 6.4 ± 0.5 nm Rh nanocubes were obtained at 105 (Figure 6a), 125 (Figure 6b), 145 (Figure 6c), 165, and 185 °C (Figures 5c,S1d), respectively. Interestingly, the cube selectivity increased from 37% at 105 °C, to 62% at 125 °C, and to 87% at 145 °C (Figure 6d). From 145 to 185 °C, the cube selectivity was sustained at a value around 85% (Figure 6d), and the nanocubes showed straight edges and sharp corners (Figures 5c and 6c). This indicates that the reactions at relatively high temperatures enhance the cube selectivity, and help to develop well-shaped nanocubes.

4. Shape Control Mechanism of (111) and (100)-Oriented Rh Nanocrystals.

13
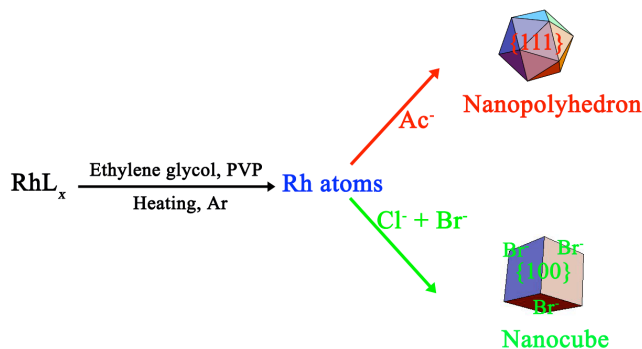
Figure 7. A schematic illustration of the reaction pathways responsible for the formation of (111) and (100)-oriented Rh nanocrystals.

Generally, shape control of noble metals is conducted by thermodynamic or kinetic control by tuning the ratio of growth rates along the <111> and <100> directions in various solution phase synthesis via selective adsorption of selective chemical species on a specific crystal plane.[1-7,9] As is known, for fcc metals, the order of surface energy for different crystal planes is (111) < (100) < (110), thus the (111) surface is the most stable one. Since (111) twinned particles have the lowest free energy, they are thermodynamically favored for fcc noble metals.[10] Recently, using $Rh(acac)_3$ as the precursor, we obtained size-tunable (5-15 nm) PVP-capped monodisperse Rh polygonal nanocrystals with the (111) surface structure by a one-step polyol reduction in 1,4-butanediol at temperatures of 170-230 °C under Ar.[9] The nanocrystals are composed of hexagons, pentagons and triangles in 2D projection (>65% in yield), among which, thermodynamically-favored twinned particles (hexagons and pentagons) showed a selectivity greater than 45%. In the present work, employing $[(Rh(ac)_2)_2]$ as the precursor, we obtained Rh nanopolyhedra dominated by (111)-oriented twinned particles in ethylene glycol at temperatures of 125-185 °C (Figure 7). In these two approaches, the decomposition of organic ligands in the precursor complexes does not produce strong surface selective adsorbates during the reaction process. As a result, Rh nanocrystals with (111) surface structure were formed, and their sizes were gradually increasing with the reaction temperature from 125 to 185 °C (see Figure 4d).

14
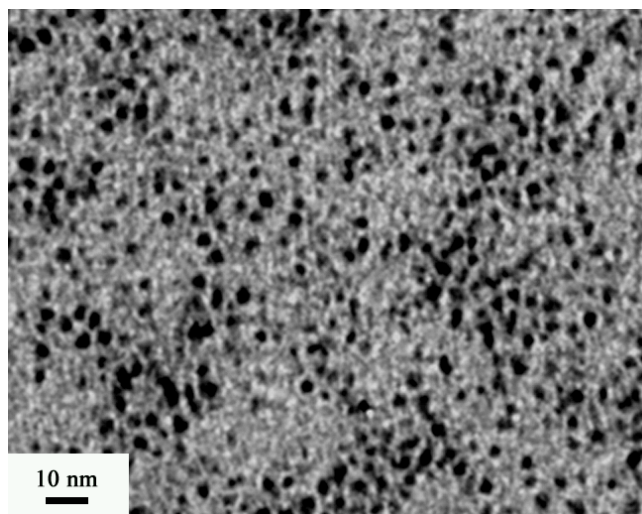
Figure 8. TEM image of Rh nanocrystals synthesized in 20 ml ethylene glycol under an Ar atmosphere at 165 °C for 1.5 h, using 2.5 mM [Rh(Ac)$_2$]$_2$, 5 mM TMAB, and 50 mM PVP.

Experimentally, we found that the reduction of RhCl$_3$, [(Rh(ac)$_2$)$_2$] and Rh(acac)$_3$ by ethylene glycol started at around 105 °C, 125 °C and 165 °C, respectively. By monitoring the time of the color change from Rh precursors (light yellow for RhCl$_3$, green for [(Rh(ac)$_2$)$_2$], and orange yellow for Rh(acac)$_3$) to Rh nanocrystals (black), we found that, at a given temperature, the reduction rates of the precursors follow the trend of RhCl$_3$ > [(Rh(ac)$_2$)$_2$] >> Rh(acac)$_3$. Using these three precursors, (111)-oriented Rh nanocrystals were formed (Figure 3a,b,c) regardless of the reduction rates of the precursors and the reaction temperatures tested (Figure 4a-c). Thus, (111)-oriented Rh nanocrystals are indeed favored by thermodynamics under conditions where no strongly chemically adsorbed species form on the surface of Rh nanocrystals during crystal growth. However, for these three precursor compounds, monodisperse Rh nanocrystals were only obtained in the case of [(Rh(ac)$_2$)$_2$], possibly due to a balance between nucleation and growth stages achieved in the reduction of [(Rh(ac)$_2$)$_2$] by ethylene glycol.[2c,d,9]

Further experiments confirmed that the introduction of Br$^-$ ions into the polyol reaction can effectively stabilize the (100) plane of Rh nanocrystals, since Br$^-$ ions tend to be more strongly adsorbed on the (100) plane than on the (111) plane (Figure 7).[1g] Under this condition, (100)-oriented nanocubes in a high selectivity were formed (Figures 1b, 3d, and 5), and the size of the nanocubes nearly remains a constant

value of around 6.5 nm despite of the elevated reaction temperatures from 105 to 185 °C because of the rigid growth restriction of the {100} facets by the strong adsorption of Br⁻ ions on them during the synthesis (see Figure 6d). However, in the absence of Cl⁻ ions, poorly-faceted cube-like Rh nanocrystals were formed (Figure 3d),[1g] indicating that the presence of Cl⁻ ions assists in developing well-defined Rh nanocubes (Figures 5 and 6a-c). In addition, we found that the reaction of $[Rh(Ac)_2]_2$ in the presence of TMAB produced small, irregular and polydisperse Rh nanoparticles (4.1±0.9 nm; Figure 8). Therefore, we concluded that monodisperse Rh nanocubes were only formed when $RhCl_3$ and alkylammonium bromide were used as the metal precursor and Br⁻ source, respectively (Figure 7).

From UV-vis spectroscopic measurements, we knew that PVP displays a very strong absorption peak at 208 nm, and $RhBr_3$ has a weak absorption band at 275 nm; while $RhCl_3$ has no clear absorption at 275 nm (Figure 9). Using $RhCl_3$ and TTAB as the reactants, the appearance of a band at 275 nm after the reaction solution has been evacuated at 80 °C for 20 min (Figure 9), indicates that $[(C_{14}H_{29})(CH_3)_3N]^+[RhCl_{4-x}Br_x]$ complexes probably form under these conditions.[3c,11] As the temperature was increased above 100 °C, the band at 275 nm disappeared (Figure 9) and the color changed from dark brown to black, indicating the complete reduction of Rh monomers. From further TEM characterizations, we knew that 6.2 ± 0.5 nm Rh nanocubes in a selectivity of 47% were formed at 105 °C (Figure 6a), indicating that there exists strong bonding interactions between the Rh nuclei and Br⁻ ions from alkylammonium bromide in the reaction solution. During the nanocube growth process, chemically adsorbed Br⁻ species not only stabilize the (100) face, but also restrain the particle growth rate. Therefore, the use of different alkylammonium bromides produced sub-10 nm sized Rh nanocubes, all in sizes close to 6.5 nm, regardless of the hydrocarbon chain length of the surfactants and the reaction temperatures. Furthermore, the formation of Rh nanocubes between 105 to 185 °C by the addition of alkylammonium bromide in the polyol reduction suggests that Rh nanocubes are the thermodynamically-favored products under these conditions.
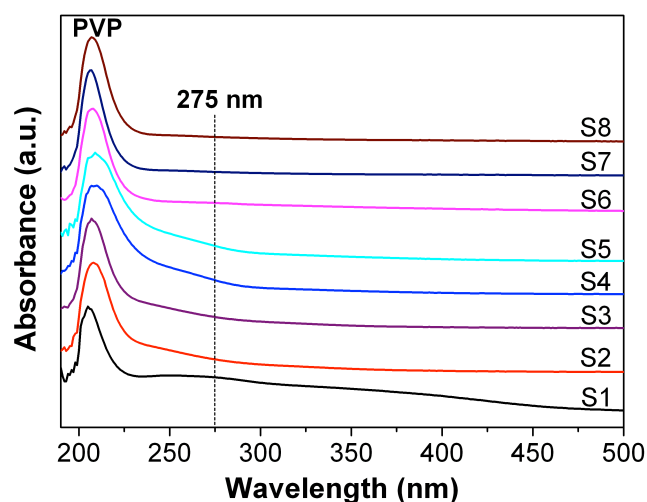
Figure 9. UV-Vis spectra of the Rh samples taken at different conditions: **S1**: ethylene glycol solution containing $RhBr_3$ and PVP; **S2**: ethylene glycol solution containing $RhCl_3$ and PVP; **S3:** ethylene glycol solution containing 10 mM $RhCl_3$, 50 mM TTAB and 200 mM PVP without further processing; **S4:** sample taken from the reaction solution (ethylene glycol solution containing 10 mM $RhCl_3$, 50 mM TTAB and 200 mM PVP) after 20 min evacuation at 80 °C; **S5**: sample taken from the reaction solution at 100 °C; **S6**: sample taken from the reaction solution at 185 °C; **S7**: sample taken from the reaction solution after 45 min at 185 °C; **S8**: sample taken from the reaction solution after 1.5 h at 185 °C.

5. CO-O_2 Reactions with (111) and (100)-Oriented Rh Nanocrystals.

With a LB trough, the as-obtained 6.5 nm Rh nanopolyhedra and nanocubes were deposited onto silicon wafers to form 2D catalytic nanoarray monolayers, which were then tested for CO oxidation activity between 170 and 230 °C. Four (111) and (100)-oriented Rh nanocatalysts at a constant size of ~ 6.5 nm were synthesized by our seedless polyol method, and were denoted as **Rh-1** (0.3125 mM $[Rh(Ac)_2]_2$ and 12.5 mM PVP in 20 ml ethylene glycol under Ar at 185 °C for 2 h), **Rh-2** (0.625 mM $Rh(acac)_3$ an 6.25 mM PVP in 1,4-butanediol under Ar at 225 °C for 2 h),[9] **Rh-3** (10 mM $RhCl_3$, 50 mM TMAB and 200 mM PVP in 20 ml ethylene glycol under Ar at 185 °C for 1.5 h), and **Rh-4** (10 mM $RhCl_3$, 50 mM TTAB and 200 mM PVP in 20 ml ethylene glycol under Ar at 185 °C for 1.5 h)**.** Turnover frequency (TOF) was calculating by extrapolating the conversion data to the initial time and by correcting the Rh surface area for coverage from

17

TEM and SEM, and for shape (assuming non-overlapping cubic particles). The SEM measurements indicated that the as-deposited Rh nanocrystals in the monolayer remain intact and do not aggregate before and after reaction.[13] For the samples of **Rh-1**, **Rh-2**, **Rh-3**, and **Rh-4**, the geometric sizes were 6.5±0.6, 6.3±0.6, 6.2±0.6, and 6.4±0.5 nm, respectively, and the numbers of the calculated surface Rh atoms were 2.9×10^{15}, 2.3×10^{15}, 4.4×10^{15}, and 3.9×10^{15}, respectively. The combined results from X-ray photoelectron spectroscopy (XPS) and energy dispersive X-ray analysis (EDAX) have demonstrated that PVP molecules were more strongly adsorbed to the Rh nanocube surfaces after washing treatment and a small fraction of Br species were present on the nanocube surfaces along with the PVP molecules.[1g]

Catalytic tests have demonstrated that all the four catalysts were active for the $CO-O_2$ reaction between 170 and 230 °C. At 200 °C, the turnover frequencies (TOF) of **Rh-1**, **Rh-2**, **Rh-3**, and **Rh-4** (Ref. 1g) are 5.5, 4.3, 3.9, and 2.1 s^{-1} (Table 1), respectively, comparable to those reported for Rh(111) and Rh(100) single crystals.[12] For the $CO-O_2$ reaction, **Rh-1**, **Rh-2**, **Rh-3**, and **Rh-4** have apparent activation energies of 30, 32, 31 and 35 kcal mol^{-1} (Table 1), respectively, indicating that this reaction is structure insensitive for the as-obtained 6.5 nm (111)-orientated Rh nanopolyhedra and (100)-oriented nanocubes, just the same as that observed for Rh(111) and Rh(100) single crystals.[1g,12] However, presumably owing to the adsorption of capping ligands on the nanocrystal surfaces, the four Rh nanocatalysts show somewhat higher apparent activation energies for CO oxidation than those (25.4 kcal mol^{-1}) reported for Rh(111) and Rh(100) single crystals.[12] More recently, we have found a shape dependent selectivity in the reduction of NO by CO with the as-prepared (111)-orientated Rh nanopolyhedra and (100)-oriented nanocubes.[14]

Conclusions

We have developed a selective synthesis of monodisperse PVP-capped sub-10 nm (6.5 nm) Rh nanocrystals with (111) and (100) surface structures, through a seedless polyol reduction in ethylene glycol. The (111)-oriented Rh nanopolyhedra dominated by (111)-twined hexagons (observed in 2D projection) were synthesized using [Rh(Ac)$_2$]$_2$ as the metal precursor; whereas, the (100)-oriented Rh nanocubes were obtained in the presence of alkylammonium bromides (e.g., tetramethylammonium bromide, trimethyl(tetradecyl)ammonium bromide), employing RhCl$_3$ as the metal precursor. The evolution of Rh

nanocubes was induced from the effective stabilization of {100} faces by chemically adsorbed Br⁻ ions from alkylammonium bromides. The (111)-oriented Rh nanopolyhedra and (100)-oriented Rh nanocubes were deposited onto silicon wafers to form 2D model nanoarray catalysts with a Langmuir-Blodgett trough. Catalytic measurements showed that these nanocatalysts were active for CO-O$_2$ reaction, and the turnover frequency is structure insensitive, in agreement with previous findings for Rh(111) and Rh(100) single crystals.

Supporting Information Available: More TEM images of as-synthesized Rh nanocrystals (Figure S1) are included in supporting information. This material is available free of charge via the Internet at http://pubs.acs.org.

References and Notes

(1) (a) Ahmadi, T. S.; Wang, Z. L.; Green, T. C.; Henglein, A.; El-Sayed, M. A. *Science* **1996**, *272*, 1924. (b) Tian, N.; Zhou, Z. Y.; Sun, S. G.; Ding, Y.; Wang, Z. L. *Science* **2007**, *316*, 732. (c) Bratlie, K. M.; Lee, H., Komvopoulos, K.; Yang, P.; Somorjai; G. *Nano Lett.* **2007**, *7*, 3097. (d) Habas, S. E.; Lee, H.; Radmilovic, V.; Somorjai, G. A.; Yang, P. *Nature Mater.* **2007**, *6*, 692. (e) Lee, H.; Susan, E. H.; Somorjai, G. A.; Yang, P. *J. Am. Chem. Soc.* **2008**, *130*, 5406. (f) Wang, C.; Daimon, H.; Onodera, T; Koda, T.; Sun, S. *Angew. Chem. Int. Ed.* **2008**, *47*, 3588. (g) Zhang, Y.; Grass, M. E.; Kuhn, J. N.; Tao, F.; Habas, S. E.; Huang W.; Yang, P.; Somorjai, G. A. *J. Am. Chem. Soc.* **2008**, *130*, 5868. (h) Nolte, P.; Stierle, A.; Jin-Phillipp, N. Y.; Kasper, N.; Schulli, T. U.; Dosch, H. *Science* **2008**, *321*, 1654. (i) Somorjai, G. A.; Park, J. Y. *Angew. Chem. Int. Ed.* **2008**, *47*, 9212. (j) Somorjai, G. A.; Frei, H., Park, J. Y. *J. Am. Chem.* Soc. **2009,** *131*, 16589. (k) Tsung, C.-K.; Kuhn, J. N.; Huang, W.; Aliaga, C.; Hung, L.; Somorjai, G. A.; Yang, P. *J. Am. Chem. Soc.* **2009**, *131*, 5816. (l) Zeng, J.; Zhang, Q.; Chen, J.; Xia, Y. *Nano Lett.* **2010**, *10*, 30.

(2) (a) Narayanan, R.; El-Sayed, M. A. *J. Phys. Chem. B* **2005**, *109*, 12663. (b) Somorjai, G. A.; Park, J. Y. *J. Chem. Phys.* **2008**, *128*, 182504. (c) Tao, A. R.; Habas, S.; Yang, P. *Small* **2008**, *4*, 310. (d) Xiong, Y.; Xia, Y. *Adv. Mater.* **2007**, *19*, 3385.

(3) (a) Song, H.; Kim, F.; Connor, S.; Somorjai, G. A.; Yang, P. *J. Phys. Chem. B* **2005**, *109*, 188. (b) Chen, J.; Herricks, T.; Xia, Y. *Angew. Chem. Int. Ed.* **2005**, *44*, 2589. (c) Lee, H.; Habas, S. E.; Kweskin, S., Butcher, D.; Somorjai, G. A.; Yang, P. *Angew. Chem. Int. Ed.*, **2006**, *45*, 7824.

(4) (a) Xiong, Y.; Chen, J.; Benjamin, J. W.; Xia, Y.; Aloni, S.; Yin, Y. *J. Am. Chem. Soc.* **2005**, *127*, 7332. (b) Xiong, Y., McLellan, J. M.; Yin, Y; Xia, Y. *Angew. Chem. Int. Ed.* **2007**, *46*, 790. (c) Xiong, Y.; Cai, H.; Wiley, B. J.; Wang, J.; Kim, M. J.; Xia, Y. *J. Am. Chem. Soc.* **2007**, *129*, 3665.

(5) (a) Tao, A.; Sinsermsuksakul, P.; Yang, P. *Angew. Chem. Int. Ed.* **2006**, *45*, 4597. (b) Chen, S; Carroll, D. L. *J. Phys. Chem. B* **2004**, *108*, 5500.
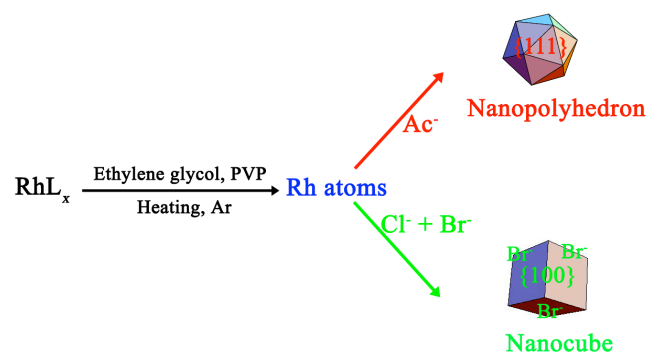
(6) (a) Seo, D.; Park, J. C.; Song, H. *J. Am. Chem. Soc.* **2006**, *128*, 14863. (b) Wu, H.-Y.; Liu, M.; Huang, M. H. *J. Phys. Chem. B* **2006**, *110*, 19291.

(7) (a) Zettsu, N.; McLellan, J. M.; Wiley, B.; Yin, Y.; Li, Z.-Y.; Xia, Y. *Angew. Chem. Int. Ed.* **2006**, 45, 1288. (b) Humphrey, S. M.; Grass, M. E.; Habas, S. E.; Niesz, K.; Somorjai, G. A.; Tilley, T. D., *Nano Lett.* **2007**, *7*, 785. (c) Hoefelmeyer, J. D.; Niesz, K.; Somorjai, G. A.; Tilley, T. D. *Nano Lett.* **2005**, *5*, 435. (d) Park, K. H.; Jang, K.; Kim, H. J.; Son, S. U. *Angew. Chem. Int. Ed.* **2007**, *46*, 1152. (e) Jang, K.; Kim, H. J.; Son, S. U. *Chem. Mater.* **2010**, *22*, 1273. (f) Kundu, S.; Wang, K.; Liang, H. *J. Phys. Chem. C* **2009**, *113*, 18570.

(8) (a) Pellegatta, J.-L.; Blandy, C.; Collière, V.; Choukroun, R.; Chaudret, B.; Cheng P.; Philippot, K. *J. Mol. Catal. A* **2002**, *178*, 55. (b) Yoon, T.-J.; Kim, J. I.; Lee J.-K. *Inorg. Chim. Acta* **2003**, *345*, 228. (c) Halttunen, M. E.; Niemelä, M. K.; Krause, A.O.I.; Vaara, T.; Vuori, A.I. *Appl. Catal. A* **2001**, *205*, 37. (d) Gayen, A.; Baidya, T.; Biswas, K.; Roy, S.; Hegde, M.S. *Appl. Catal. A* **2006**, *315*, 135. (e) Pan H.-B.; Wai, C. M. *J. Phys. Chem. C* **2009**, *113*, 19782.

(9) Zhang, Y.; Grass, M. E.; Habas, S. E.; Tao, F.; Zhang, T.; Yang, P.; Somorjai, G. A. *J. Phys. Chem. C* **2007**, *111*, 12243.

(10) (a) Wang, Z. L. *J. Phys. Chem. B* **2000**, *104*, 1153. (b) Marks, L. D. *Rep. Prog. Phys.* **1994**, *57*, 603.

(11) Veisz, B.; Király, Z. *Langmuir* **2003**, *19*, 4817.

(12) Peden, C. H. F.; Goodman, D. W.; Blair, D. S.; Berlowitz, P. J.; Fisher, G. B.; Oh, S. H. *J. Phys. Chem.* **1988**, *92*, 1563.

(13) Grass, M. E.; Zhang, Y.; Butcher, D. R.; Park, J. Y.; Li, Y.; Bluhm, H.; Bratlie, K. M.; Zhang, T.; Somorjai, G. A. *Angew. Chem. Int. Ed.* **2008**, *47*, 8893.

(14) Renzas, J. R.; Zhang, Y.; Huang, W.; Somorjai, G. A. *Catal. Lett.* **2009**, *132*(3-4), 317.

TABLE 1: CO-O$_2$ Turnover Frequency (TOF), Activation Energy (Ea) for the LB Monolayers of (111) and (100) Oriented Rh Nanocrystals on Silicon Wafers

	Shape	Size (nm)	Orientation	Coverage[a]	Ea (kcal mol^{-1})	TOF[b] at 200 °C (s^{-1})
Rh-1	Polyhedron	6.5±0.6	(111)	0.37	30	5.5
Rh-2[c]	Polyhedron	6.3±0.6	(111)	0.19	32	4.3
Rh-3	Cube	6.2±0.6	(100)	0.56	31	3.9
Rh-4	Cube	6.4±0.5	(100)	0.39	35	2.1 (Ref. 1g)

[a] Coverage determined from a 1 μm × 1 μm area of a TEM grid lifted from LB trough. [b] Surface Rh atoms were determined from geometric considerations. Reaction conditions were 40 Torr CO, 100 Torr O$_2$, 170-230 °C. [c] Prepared from 0.625 mM Rh(acac)$_3$ and 6.25 mM PVP in 1,4-butanediol under Ar at 225 °C for 2 h.[9]

Table of Contents

$$RhL_x \xrightarrow[\text{Heating, Ar}]{\text{Ethylene glycol, PVP}} \text{Rh atoms}$$

Ac⁻

{111}

Nanopolyhedron

Cl⁻ + Br⁻

Br⁻ Br⁻
{100}
Br⁻

Nanocube

LEGAL DISCLAIMER